Applied Radiation and Isotopes 104 (2015) 224–231

Contents lists available at ScienceDirect

Applied Radiation and Isotopes

journal homepage: www.elsevier.com/locate/apradiso

Pulse height tests of a large diameter fast $LaBr_3$:Ce scintillation detector

A.A. Naqvi [a,*], F.Z. Khiari [a], M. Maslehuddin [b], M.A. Gondal [a], O.S.B Al-Amoudi [c], M.S. Ukashat [a], A.M. Ilyas [a], F.A. Liadi [a], A.A. Isab [d], Khateeb-ur Rehman [a], M. Raashid [a], M.A. Dastageer [a]

[a] Department of Physics, King Fahd University of Petroleum and Minerals, Dhahran, Saudi Arabia
[b] Center for Engineering Research, King Fahd University of Petroleum and Minerals, Dhahran, Saudi Arabia
[c] Department of Civil and Environmental Engineering, King Fahd University of Petroleum and Minerals, Dhahran, Saudi Arabia
[d] Department of Chemistry, King Fahd University of Petroleum and Minerals, Dhahran, Saudi Arabia

HIGHLIGHTS

- Pulse height tests of 100 mm × 100 mm cylindrical fast $LaBr_3$:Ce detector.
- Prompt gamma ray measurements.
- Water samples with mercury (3.1 wt%), boron (2.5 wt%), cadmium (0.25 wt%), chromium (52 wt%), and nickel (22 wt%) contamination.

ARTICLE INFO

Article history:
Received 2 June 2015
Received in revised form
1 July 2015
Accepted 10 July 2015
Available online 11 July 2015

Keywords:
$LaBr_3$:Ce detector pulse height tests
Prompt gamma rays detection
Mercury
Boron
Nickel
Cadmium and Chromium contaminated water samples
Portable neutron generator based PGNAA setup

ABSTRACT

The pulse height response of a large diameter fast 100 mm × 100 mm $LaBr_3$:Ce detector was measured for 0.1–10 MeV gamma-rays. The detector has a claimed time resolution of 608 ps for 511 keV gamma rays, but has relatively poor energy resolution due to the characteristics of its fast photomultiplier. The detector pulse height response was measured for gamma rays from cobalt, cesium, and bismuth radioisotope sources as well as prompt gamma rays from thermal neutron capture in water samples contaminated with mercury (3.1 wt%), boron (2.5 wt%), cadmium (0.25 wt%), chromium (52 wt%), and nickel (22 wt%) compounds. The energy resolution of the detector was determined from full width at half maximum (FWHM) of element-characteristic gamma ray peaks in the pulse height spectrum associated with the element present in the contaminated water sample. The measured energy resolution of the 100 mm × 100 mm detector varies from 12.7 ± 0.2% to 1.9 ± 0.1% for 0.1 to 10 MeV gamma rays, respectively. The graph showing the energy resolution $\Delta E/E(\%)$ versus $1/\sqrt{E_\gamma}$ was fitted with a linear function to study the detector light collection from the slope of the curve. The slope of the present 100 mm × 100 mm detector is almost twice as large as the slope of a similar curve of previously published data for a 89 mm × 203 mm $LaBr_3$:Ce detector. This indicates almost two times poorer light collection in the 100 mm × 100 mm detector as compared to the other detector.

1. Introduction

Recently developed lanthanide-based gamma ray detectors have excellent energy and time resolutions (Favalli et al., 2010; Van Loef et al., 2001). They have high potential for applications in studies involving pulse height spectroscopy (Camera et al., 2014; Giaz et al., 2013; Menge et al., 2007; Naqvi et al., 2011, 2012a, 2012b; Owens et al., 2007) and timing analysis (Iltisa et al., 2006; Kuhn et al., 2004, 2005, 2006; Surti et al., 2003). Detectors designed for pulse height spectroscopy are coupled to photomultipliers with excellent energy resolution while those designed for timing analysis have their scintillator crystals coupled to fast photomultipliers with excellent time resolution (Iltisa et al., 2006; Kuhn et al., 2005). Fast photomultipliers have relatively poor energy resolution while spectroscopy photomultipliers have poor time resolution (Kuhn et al., 2004, 2006; Modamio et al., 2015; Surti et al., 2003). Furthermore, the time resolution of $LaBr_3$:Ce detectors also depends upon the $LaBr_3$:Ce crystal size and its cerium doping concentration, better time resolution with higher

* Corresponding author.

http://dx.doi.org/10.1016/j.apradiso.2015.07.009
0969-8043/

cerium doping concentration (Iltisa et al., 2006; Kuhn et al., 2005, 2006). The energy resolution of the $LaBr_3$:Ce detector deteriorates with increasing cerium doping due to optical self-absorption of cerium. Due to higher cerium concentration of $CeBr_3$ detectors than $LaBr_3$:Ce detectors, $CeBr_3$ detector has poorer resolution of 4.4% as compared to 2.9% measured for $LaBr_3$:Ce detector for 661 keV gamma rays (Weele et al., 2014). As the detector volume increases its time resolution deteriorates but its detection efficiency for higher energy gamma rays improves. Additional large diameter detectors offer larger solid angles resulting in reduced counting times in the experiments. The energy and time resolutions of large volume $LaBr_3$:Ce detectors were previously measured (Giaz et al., 2013). For 76 mm × 76 mm (diameter × height) and 90 × 203 mm^2 (diameter × height) $LaBr_3$:Ce detectors, the measured energy resolutions were 3.0–3.1% for 661 keV gamma rays; but the reported time resolutions of these detectors for 511 keV gamma rays were 671 and 880 ps, respectively (Giaz et al., 2013).

A large diameter 100 mm × 100 mm (diameter × height) $LaBr_3$:Ce detector has been acquired by King Fahd University of Petroleum and Mineral for the time-flight spectroscopy program. Large volume $LaBr_3$:Ce detectors designed for timing spectroscopy are coupled to fast photomultipliers which have relatively poor energy resolution. In this study the energy resolution of the large diameter $LaBr_3$:Ce detector was measured for gamma-rays with energies up to 10.0 MeV. The findings of this study are reported in this paper.

2. Experimental methods

2.1. Measurement of the detector intrinsic activity

The $LaBr_3$:Ce detector (with 100 mm × 100 mm $LaBr_3$:Ce crystal, coupled to a fast photomultiplier model number R4144) was supplied to us by the manufacturer Saint Gobain, France, as a single unit along with a matching voltage divider. The detector was operated at negative 994 V voltage. The detector body has a common ground connection with dynode and timing output with grounded-anode configuration of the photomultiplier. The detector time resolution warranted by the manufacturer for 511 keV gamma rays was 608 ps. In the present study, the time resolution of the 100 mm × 100 mm detector was not measured. The manufacturer-quoted time resolution of our detector is better than the time resolution for a 89 mm × 203 mm $LaBr_3$:Ce detector reported earlier (Giaz et al., 2013). The energy resolution of the 100 mm × 100 mm $LaBr_3$:Ce detector quoted by the manufacturer for 661 keV gamma rays was 5.3%.

The intrinsic activity of the 100 mm × 100 mm detector was determined using the procedure described for the smaller 76 mm × 76 mm $LaCl_3$:Ce (Naqvi et al., 2012a, 2012b) and $LaBr_3$:Ce detectors (Naqvi et al., 2011). The activity/second was determined from the area under the 1468 keV peak of the detector as shown in Fig. 1. The lack of a bend on the lower slope of the 1468 keV peak in this spectrum (as observed in other smaller sizes $LaBr_3$:Ce detectors) is due to poorer energy resolution of the detector caused by the coupled fast photomultiplier with poorer energy resolution. The detector activity was measured for 101 s and was found to be 142 ± 1 counts/s. The photopeak efficiency (PE) of the large detector was calculated from the ratio of the measured activity count rate (142 ± 1 counts/s) and the calculated activity of 775 Bq for a 100 mm × 100 mm LaBr detector. The PE of the large detector was found to be 0.183. The activity of the 100 mm × 100 mm LaBr detector was calculated from extrapolation of Menge et al. data for smaller sizes $LaBr_3$:Ce detectors to 100 × 100 mm^2 LaBr detector. For smaller cylindrical $LaBr_3$:Ce detectors of 38 mm × 38 mm,

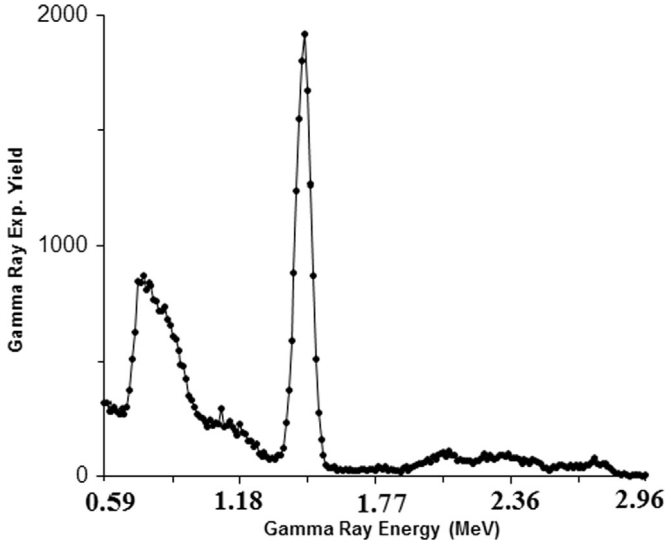

Fig. 1. 100 mm × 100 mm $LaBr_3$:C detector intrinsic activity pulse height spectrum exhibiting 1468 keV line from lanthanum.

41 mm × 76 mm, and 51 mm × 76 mm sizes (diameter × height), Menge et al. reported calculated activity of the detector for 1436 + 32 keV as 42.6 Bq, 99.0 Bq, and 153 Bq, respectively. They also reported photopeak count rates (count/s) for expected/measured count rates for theses detectors as (3.32/3.55), (10.7/10.6) and (21.1/21.8), respectively. From the ratio of measured count rate and calculated activity, the photopeak efficiency was derived (Menge et al., 2007). Previously, the PE of the 76 mm × 76 mm $LaBr_3$:Ce and $LaCl_3$:Ce detectors were reported to be 0.191 (Naqvi et al., 2012a) and 0.16 (Naqvi et al., 2012b), respectively.

The energy resolution of the large $LaBr_3$:Ce detector was measured for 662 keV gamma-rays from ^{137}Cs source. The pulse height spectrum of the large detector from ^{137}Cs source is shown in Fig. 2. For 662 keV gamma-rays, the energy resolution of the detector was measured to be 5.8%. This is 9% higher than the manufacturer's warranted energy resolution (5.3%) of the detector.

2.2. Measurement of $LaBr_3$:Ce detector activation spectrum

The gamma-ray tests of the large detector were performed following the method used for the smaller lanthanum-halide

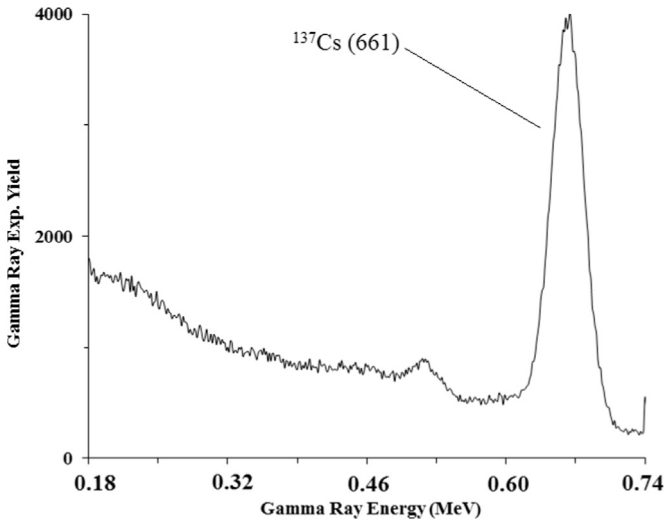

Fig. 2. $LaBr_3$:Ce pulse height spectrum taken with ^{137}Cs source exhibiting 662 keV peak.

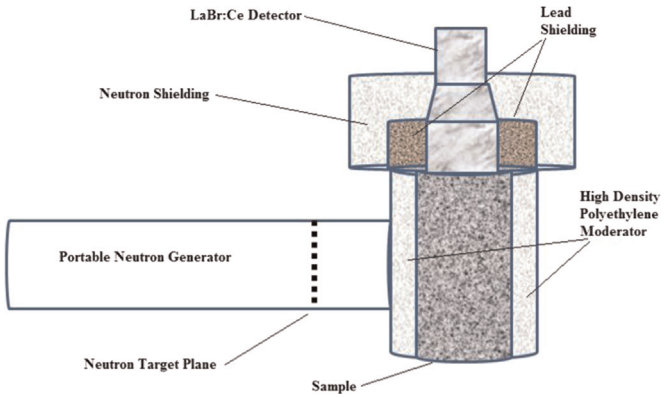

Fig. 3. Schematic representation (not to the scale) of the portable neutron generator-based PGNAA setup used in the prompt gamma-ray tests of the $LaBr_3$:C detector.

detectors (Naqvi et al., 2011, 2012a, 2012b). The tests were conducted using the PGNAA setup reported earlier (Naqvi et al., 2011, 2012a, 2012b). The setup was modified to accommodate the large $LaBr_3$:Ce detector. Fig. 3 shows a schematic drawing of the experimental setup used in the present study. Neutrons with 2.5 MeV energy from a D-D portable neutron generator are moderated in a cylindrical high density polyethylene moderator with 250 mm diameter and 140 mm height. The moderator has a 90 mm diameter central cavity drilled through to accommodate a sample bottle with an outer diameter of 90 mm and a height of 140 mm. The axis of the cylindrical sample is parallel to the neutron target plane. The large gamma-ray detector views the sample along its longitudinal axis.

The large detector is shielded against gamma rays and neutrons by 3 mm thick lead shielding and an additional 50 mm thick neutron shielding, built around the lead shield of the $LaBr_3$:Ce detector. The neutron shielding was made from mixture of paraffin and lithium carbonate (taken in equal weight proportions). The optimum sizes of the moderator and shielding were calculated using Monte Carlo simulations (Naqvi et al., 2011, 2012a, 2012b).

The detector activation spectrum was produced due to the interaction of thermal neutrons with the detector material. The activation spectrum also contains gamma ray peaks due to room background. The energies of the gamma-rays are listed in Table 1 (Choi et al., 2006).

In this study, a flux of 2.5 MeV neutrons was produced via the D (d,n) reaction using a 70 μA current deuteron beam of 70 keV energy. Due to the extended usage of the neutron generator over more than 1000 h, the neutron source strength was estimated to be 4×10^5 n/s. The beam has a frequency of 250 Hz and a pulse width of 800 μs. The detector pulse height spectra were acquired over two different energy ranges, a narrow range of 0.09–0.61 MeV for low energy capture gamma-rays from cadmium, boron and mercury and a broader energy range of 1.33–10.0 MeV for high energy gamma rays from nickel, mercury and chromium samples.

Fig. 4 shows a gamma ray spectrum of the large detector over 0.11 to 0.84 MeV energy range exhibiting prominent gamma-ray peaks of lanthanum, cerium and bromine from the detector material. The gamma ray energy data is listed in Table 1 (Choi et al., 2006).

For comparison, the activation spectrum of a smaller 76 mm × 76 mm $LaBr_3$:Ce detector (Naqvi et al., 2011) is shown in Fig. 5 over 0.05 to 2.55 MeV range. The energy resolution of the large detector is poorer as compared to the 76 mm × 76 mm $LaBr_3$:Ce detector and many peaks could not be resolved from adjacent ones. Fig. 4 shows the lanthanum peaks at 163 and 789 keV along with the bromine peaks at 196, 276, 315, 367, and 512 keV. The Ce peak at 476 keV could not be resolved from the Br peak at 512 keV and from the La peaks at 567 and 595 keV. Also, the La peak at 789 keV could not be resolved from the Br peak at 828 keV. The detector energy resolution can be calculated from the

Table 1
Energies and partial elemental cross section $\sigma_\gamma^z(E_\gamma)$-barns of prominent capture gamma-rays used in this study (Choi et al., 2006).

Element	Gamma ray energy (MeV)	$\sigma_\gamma^z(E_\gamma)$-barns
B	478	716
Br	196	0.434
	271	0.462
	275	0.158
	315	0.460
	367	0.233
	513	0.210
	661	0.082
	828	0.285
	1248	0.0527
	7577	0.108
Cd	171	57
	245	274
	558	1860
	651	359
Ce	475	0.082
	662	0.241
	1107	0.040
Hg	368	251
	5967	62.5
H	2223	0.333
Ni	8533	0.721
	8998	1.49
Cr	7099	0.146
	7938	0.424
	8483	0.169
	8511	0.233
	8884	0.780
	9719	0.260
La	163	0.489
	272	0.502
	288	0.73
	567	0.335
	595	0.103
	789	Intrinsic
	1436 + 32	Intrinsic
	2521	0.212
	5126	0.114

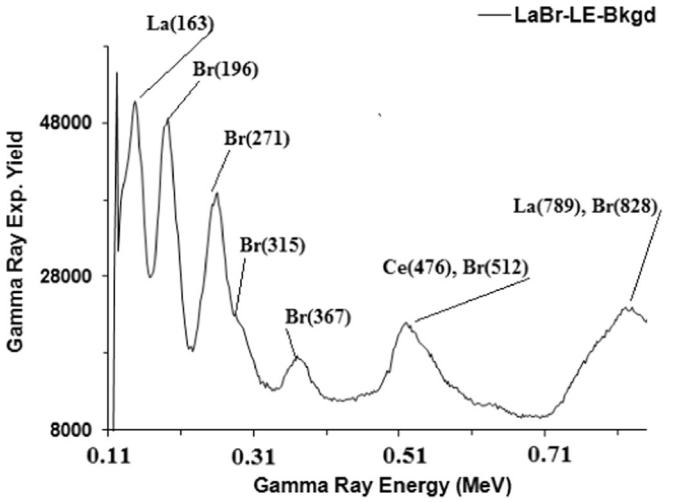

Fig. 4. Prompt gamma-ray spectrum due to activation of the 100 mm × 100 mm $LaBr_3$:Ce detector caused by capture of thermal neutrons in La, Br and Ce elements present in $LaBr_3$:Ce detector.

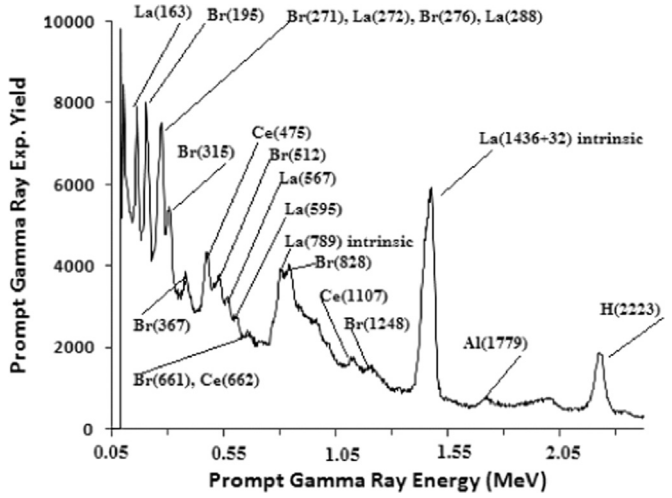

Fig. 5. Prompt gamma-ray spectrum due to activation of the 76 mm × 76 mm LaBr:Ce detector caused by capture of thermal neutrons in La, Br and Ce elements present in the $LaBr_3$:Ce detector (Naqvi et al., 2011).

activation spectrum for well resolved peaks of significant intensities.

3. Measurements of prompt gamma-ray spectra from boron-, cadmium-, mercury-, chromium-, and nickel-contaminated water samples

The spectra of the large detector were recorded from mercury-, boron-, cadmium-, chromium-, and nickel-contaminated water samples over 0.3 to 10 MeV gamma-ray energies. The detector spectra were acquired with two different energy ranges. The gamma-ray spectra from mercury, boron and cadmium were acquired over 0.09 to 0.61 MeV energy range with data acquisition time listed separately for each sample in Table 2. The gamma-ray spectra from chromium, mercury, and nickel were acquired over 1.33–10.0 MeV energy range. The mercury, boron, cadmium, chromium and nickel samples were prepared by dissolving various chemical compounds, such as boric acid, cadmium acetate, mercuric nitrate, chromium trioxide and nickel nitrate, in water and filling them in the 90 mm diameter × 145 mm long plastic (PET) bottles.

These samples were supplied by the Department of Chemistry, King Fahd University of Petroleum and Minerals, Saudi Arabia. The concentrations of the various elements along with corresponding sample measurement times are listed in Table 2. The samples' measurement times vary from 480 s to 6400 s.

Figs. 6, 8 and 10 show the detector pulse height spectra over 0.09 to 0.61 MeV gamma-rays from the mercury, boron and cadmium samples superimposed upon background spectra while Figs. 7, 9 and 11 show the background-subtracted peaks of mercury, boron and cadmium samples. In order to superimpose the sample spectra upon the background spectra, both sample and background spectra were normalized to the same counting time and same neutron flux. This was obtained by normalizing both sample and background spectra in the region where background is constant (sample independent). Then, the background spectrum was subtracted from normalized spectrum to generate the difference spectrum.

Figs. 12 and 14 show detector pulse height spectra over 1.33–10.0 MeV gamma-rays from the chromium and nickel samples while Fig. 16 shows the detector pulse height spectrum over 0.54–9.42 MeV gamma rays from the mercury sample. Figs. 13, 15 and 17 are subsections of Figs. 12, 14 and 16 showing enlarged plots of chromium, nickel and mercury peaks.

Fig. 6 shows the spectrum of mercury-contaminated water sample superimposed upon the background spectrum over 0.09 to 0.61 MeV. The mercury peak at 358 keV interferes with the

Table 2
Chemical composition and concentration of various elements samples used in the present study.

Chemical compound	Element	Concentration (wt%)	Measurement time (s)
Boric acid H_3BO_3	B	2.5	720
Cadmium acetate $Cd(CH_3CO_2)_2$	Cd	0.25	480
Mercuric nitrate $Hg(NO_3)_2$	Hg	3.1	1600
Nickel nitrate $Ni(NO_3)_2$	Ni	22	4600
Chromium trioxide CrO_3	Cr	52	6400

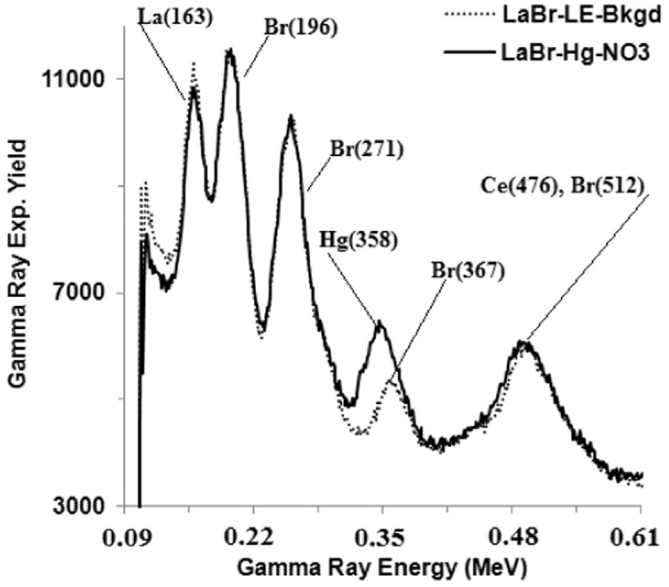

Fig. 6. Prompt gamma-rays pulse height spectra of mercuric nitrate ($NiNO_3$) contaminated water sample superimposed upon background spectrum.

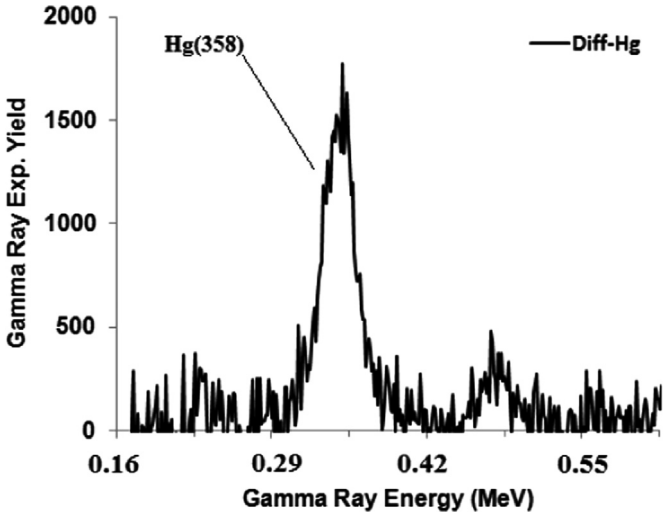

Fig. 7. Difference pulse height spectra of mercuric nitrate contaminated water sample exhibiting 358 keV mercury peak.

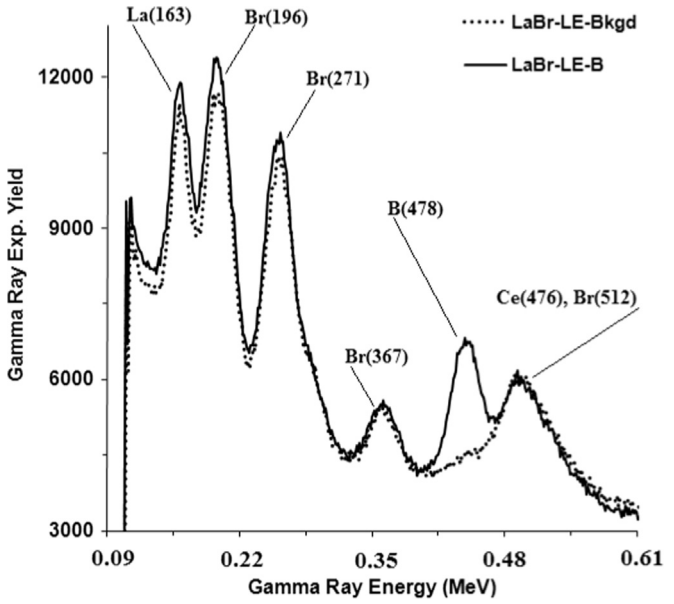

Fig. 8. Prompt gamma-rays pulse height spectra of boric acid contaminated water sample superimposed upon background spectrum.

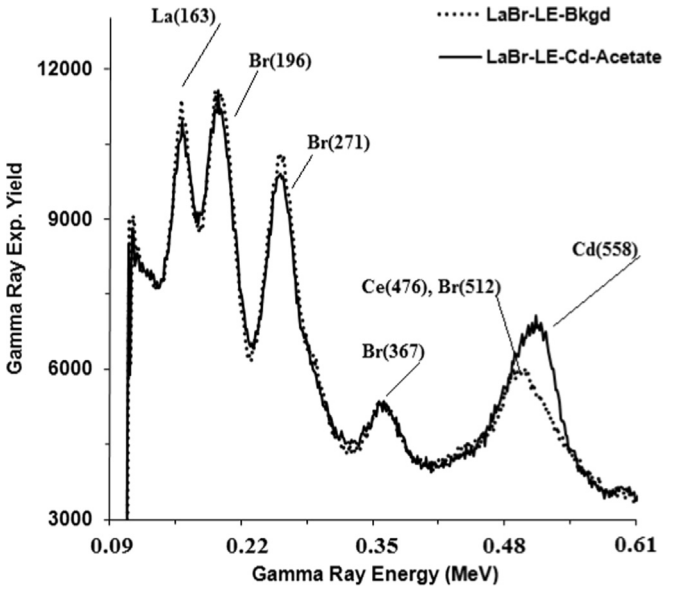

Fig. 10. Prompt gamma-rays pulse height spectra of cadmium-acetate contaminated water sample superimposed upon background spectrum.

bromine peak at 367 keV from the detector background. Fig. 7 shows the well resolved 358 keV mercury peak in the difference spectrum, obtained after subtracting background from mercury sample spectrum. Similarly, Fig. 8 shows the boron contaminated water sample spectrum superimposed upon background spectrum. The boron peak at 478 keV is interfering with cerium and bromine peaks at 476 and 512 keV, respectively. Fig. 9 shows the well resolved 478 keV boron peak in the difference spectrum, obtained after subtracting background from boron spectrum. The cadmium spectra acquired by the large detector are shown in Figs. 10 and 11. As shown in Fig. 10, the cadmium peak at 558 keV interferes with the cerium and bromine peaks at 476 and 512 keV, respectively. Fig. 11 shows the well resolved 558 keV cadmium peak in the difference spectrum, obtained after subtracting background spectrum from cadmium spectrum.

Fig. 12 shows the spectrum of chromium contaminated water sample superimposed upon the background spectrum over 1.33 to 10.0 MeV. The chromium peaks at 7099, 7938, 8884 and 9719 keV appear at the end of the spectrum. Also shown in Fig. 12, is the

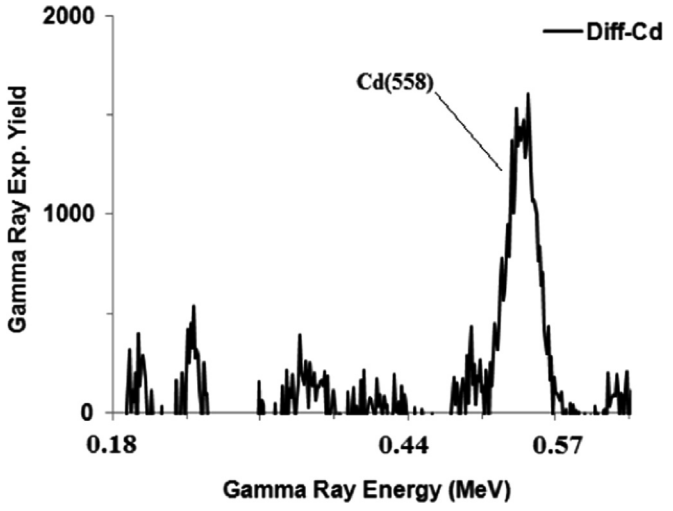

Fig. 11. Difference pulse height spectra of cadmium-acetate contaminated water sample exhibiting 558 keV cadmium peak.

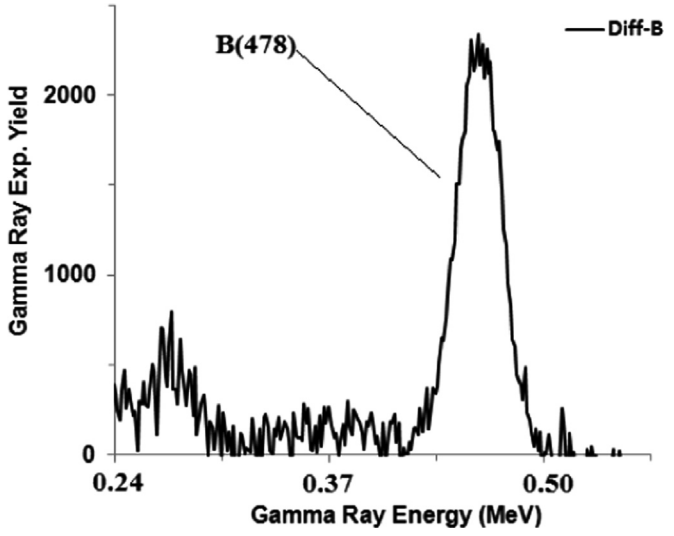

Fig. 9. Difference pulse height spectra of boric acid contaminated water sample exhibiting 478 keV boron peak.

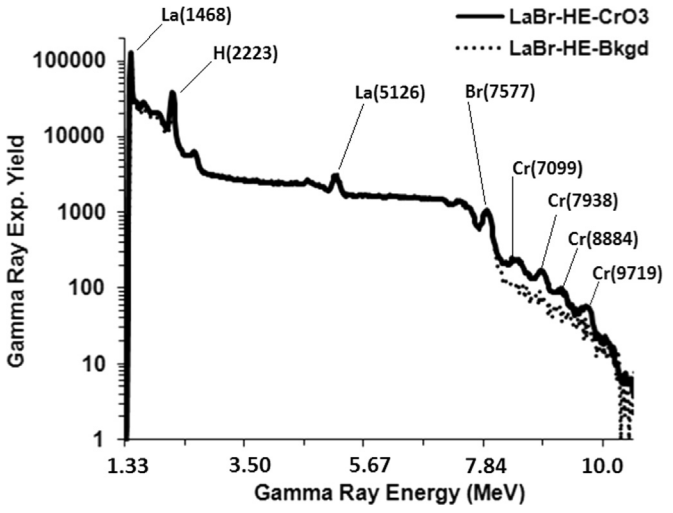

Fig. 12. Prompt gamma-rays pulse height spectra of chromium trioxide (CrO_3) contaminated water sample superimposed upon background spectrum.

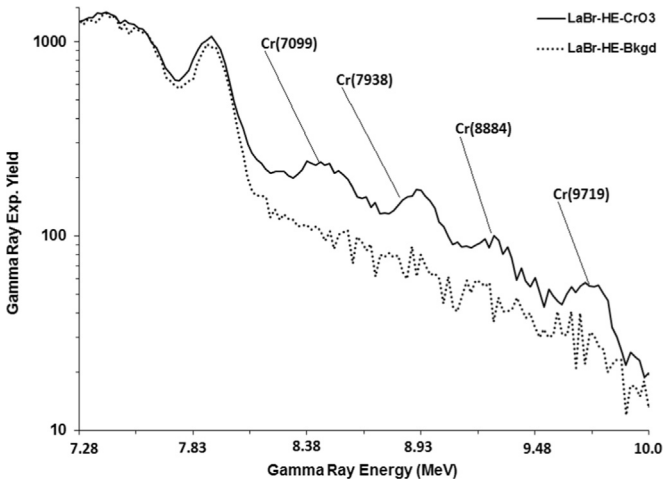

Fig. 13. Enlarged pulse height spectrum of chromium trioxide contaminated water sample exhibiting 7099, 7938, 8884 and 9719 keV chromium peaks superimposed upon background spectrum.

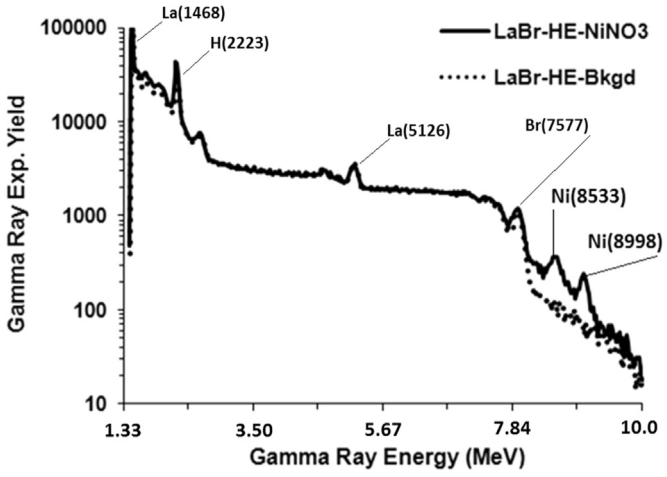

Fig. 14. Prompt gamma-rays pulse height spectra of nickel nitrate ($NINO_3$) contaminated water sample superimposed upon background spectrum.

hydrogen capture peak at 2223 keV due to capture of thermal neutrons in the high density polyethylene. The lanthanum and bromine peaks from thermal neutron capture in the detector material appear at 5126 and 7577 keV, respectively. Fig. 13 shows the enlarged part of Fig. 12 over 7.28–10.0 MeV exhibiting the chromium peaks at 7099, 7938, 8884 and 9719 keV, along with the background spectrum. Similarly, Fig. 14 shows the spectra of nickel contaminated water sample superimposed upon background spectrum over 1.33–10.0 MeV. The nickel peaks at 8533 and 8998 keV appear at the end of the spectrum. Fig. 15 shows the enlarged part of Fig. 14 over 6.77 to 10.0 MeV exhibiting the nickel peaks at 8533 and 8998 keV along with the single escape peak superimposed upon the background spectrum. The high energy gamma-ray spectrum of mercury-contaminated water sample, superimposed upon background spectrum, is shown in Fig. 16 over 0.54 to 10.0 MeV. The mercury peak could be seen at 5967 keV energy. The 5967 keV mercury peak along with its associated single escape peak, superimposed upon the background, is shown on an enlarged scale in Fig. 17.

4. Results and discussion

The gamma ray peaks data from the detector material, as well as from boron, cadmium, mercury, chromium and nickel samples

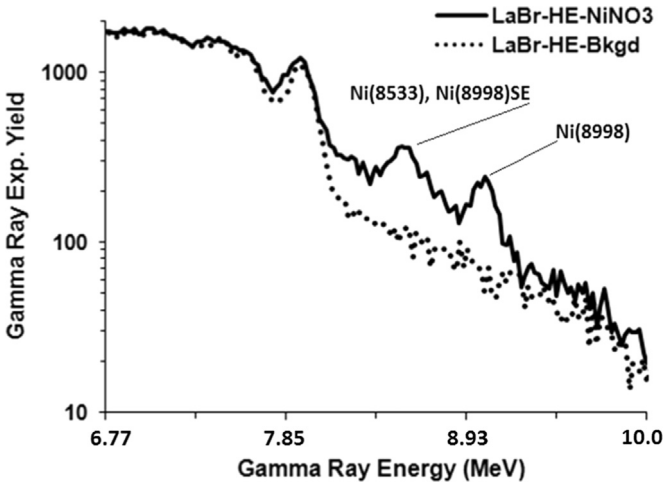

Fig. 15. Enlarged pulse height spectrum of nickel nitrate contaminated water sample exhibiting 8533 and 8998 keV nickel peaks superimposed upon background spectrum.

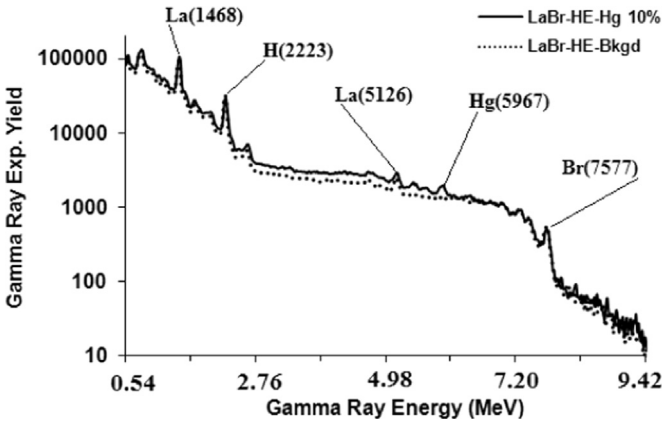

Fig. 16. Prompt gamma-rays pulse height spectra of mercuric nitrate ($HgNO_3$) contaminated water sample superimposed upon background spectrum.

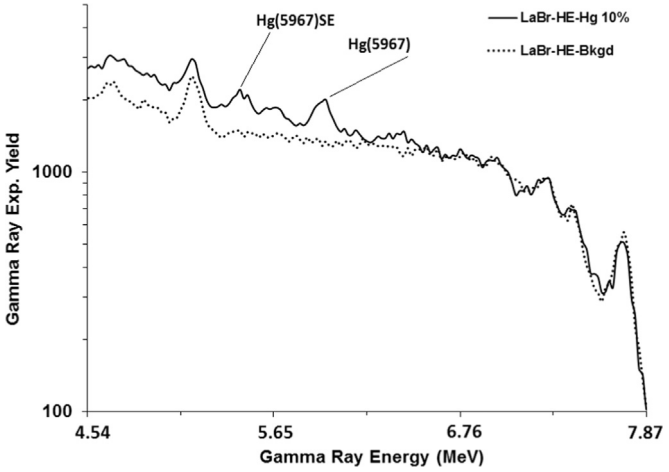

Fig. 17. Enlarged pulse height spectrum of mercuric nitrate contaminated water sample exhibiting 5967 keV mercury peak superimposed upon background spectrum.

was fitted to determine the energy resolution (FWHM) of the detector using the least squares fit method. In order to investigate the effect of light collection from the $LaBr_3$:Ce crystal, the energy

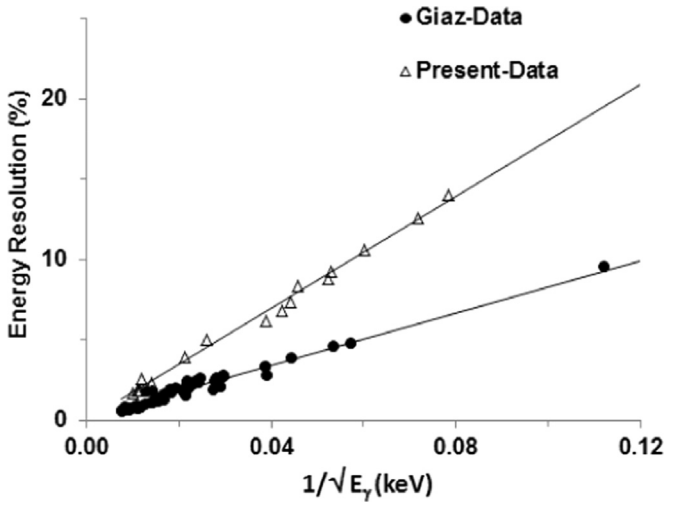

Fig. 18. Energy resolution (%) of the 100 mm × 100 mm $LaBr_3$:Ce detetor and 89 mm × 203 mm $LaBr_3$:Ce detetor (Camera et al., 2014; Giaz et al., 2013) plotted as a function of $1/\sqrt{E_\gamma}$.

Table 3
Coefficient of fit to energy resolution data of 100 mm × 100 mm and 89 mm × 203 mm $LaBr_3$:Ce detectors. (Camera et al., 2014; Giaz et al., 2013). Fitted equation: $\Delta E/E(\%) = a/(\sqrt{E_g}) + b$

Detector size	Fit coefficient	
	Coefficient *a*	Coefficient *b*
100 mm × 100 mm	174.4	0.011
89 mm × 203 mm	80.9	0.224

resolution (%) was plotted against $1/\sqrt{E_\gamma}$. The slope of the fit is indicative of the light collection of the detector assembly. For comparison, the energy resolution data of a 89 mm × 203 mm $LaBr_3$:Ce detector coupled to a photomultiplier with good energy resolution (Camera et al., 2014; Giaz et al., 2013), was also plotted against $1/\sqrt{E_\gamma}$. Since both detectors contains 5% Ce each, the only difference between them is more efficient light collection in the 89 mm × 203 mm $LaBr_3$:Ce detector (Camera et al., 2014; Giaz et al., 2013).

Fig. 18 shows the energy resolution data of the 89 mm × 203 mm $LaBr_3$:Ce and 100 × 100 mm^2 $LaBr_3$:Ce detector plotted as a function of $1/\sqrt{E_\gamma}$. The solid line through the data represents linear least squares fit to the data of the type:

$$\Delta E/E(\%) = a/(\sqrt{E_g}) + b.$$

The values of the coefficients *a* and *b* of the fit to both detectors' energy resolution data are listed in Table 3. The slope of the curve (value of coefficient *a*) for 100 mm × 100 mm detector was calculated to be 174.4 while for the 89 mm × 203 mm $LaBr_3$:Ce detector its value was 80.9. The almost two times smaller value of the slope for the 89 mm × 203 mm $LaBr_3$:Ce detector indicates almost two times better light collection for 89 mm × 203 mm $LaBr_3$:Ce detector. This is due to the fact that the photomultiplier used in the 100 × 100 mm^2 $LaBr_3$:Ce detector has poorer energy resolution but superior timing resolution. The manufacturer claimed an excellent time resolution of 608 ps for the 100 × 100 mm^2 $LaBr_3$:Ce detector as compared to 880 ps reported for the 89 mm × 203 mm $LaBr_3$:Ce detector.

5. Conclusions

Performance tests of a large diameter cylindrical 100 mm × 100 mm (height × diameter) $LaBr_3$:Ce detector were carried out for 0.10–10 MeV gamma-rays produced via thermal neutron capture in the detector material as well in mercury-, boron-, cadmium-, chromium- and nickel-contaminated water samples. From the measured gamma-ray spectra, the energy resolution of the 100 mm × 100 mm $LaBr_3$:Ce detector was derived. The percentage energy resolution data of the 100 mm × 100 mm $LaBr_3$:Ce detector was fitted as a function of $1/\sqrt{E_\gamma}$ using a linear least square fit. For comparison, previously published energy resolution data of a 89 mm × 203 mm $LaBr_3$:Ce detector (Giaz et al., 2013) was also fitted as a function of $1/\sqrt{E_\gamma}$. The difference in the slopes of the fits reveals almost twice poorer light collection from the 100 × 100 mm^2 $LaBr_3$:Ce detector. This study has provided useful data on the performance of the large fast 100 mm × 100 mm $LaBr_3$:Ce detector.

Acknowledgments

This study is part of projects #RG1008 and RG1201 funded by King Fahd University of Petroleum and Minerals, Dhahran, Saudi Arabia. The support provided by the Department of Physics, Department of Chemistry, Center for Engineering Research, and Department of Civil and Environmental Engineering at King Fahd University of Petroleum and Minerals, Dhahran, Saudi Arabia, is acknowledged.

References

Camera, F., Giaz, A., Pellegri, L., Riboldi, S., Blasi, N., Boiano, C., Bracco, A., Brambilla, S., Ceruti, S., Coelli, S., Crisp, F.C.L., Csatlòs, M., Krasznahorkay, A., Gulyàs, J., Lodetti, S., Frega, S., Miani, A., Million, B., Stuhl, L., Wieland, O., 2014. Characterization of large volume 3.5″ × 8″ $LaBr_3$: Ce detectors for the HECTOR array. In: Proceedings of INPC 2013 – International Nuclear Physics Conference, Firenze, Italy, vol. 66, Article number 11008.

Choi, H.D., Firestone, R.B., Lindstrom, R.M., Molnar, G.L., Mughabghab, S.F., Paviotti-Corcuera, R., Revay, Z., Trkov, A., Zhou, C.M., 2006. Database of Prompt Gamma-Rays from Slow Neutron Capture for Elemental Analysis. International Atomic Energy Agency, VIENNA.

Favalli, A., Mehner, H.C., Ciriello, V., Pedersen, B., 2010. Investigation of the PGNAA using the $LaBr_3$ scintillation detector. Appl. Radiat. Isot. 68, 901–904.

Giaz, A., Pellegri, L., Riboldi, S., Camera, F., Blasi, N., Boiano, C., Bracco, A., Brambilla, S., Ceruti, S., Coelli, S., Crespi, F.C.L., Csatlòs, M., Frega, S., Gulyàs, J., Krasznahorkay, A., Lodetti, S., Million, B., Owens, A., Quarati, F., Stuhl, L., Wieland, O., 2013. Characterization of large volume 3.5″ × 8″ $LaBr_3$:Ce detectors. Nucl. Instrum. Methods Phys. Res. Sect. A: Accel. Spectrom. Detect. Assoc. Equip. 729, 910–921.

Iltisa, A., Mayhughb, M.R., Mengeb, P., Rozsab, C.M., Sellesc, O., Solovyevb, V., 2006. Lanthanum halide scintillators: properties and applications. Nucl. Instrum. Methods Phys. Res. Sect. A: Accel. Spectrom. Detect. Assoc. Equip. A 563, 359–363.

Kuhn, A., Surti, S., Karp, J.S., Muehllehner, G., Newcomer, F.M., Van Berg, R., 2004. Performance Assessment of Pixelated $LaBr_3$ Detector Modules for TOF PET. In: Proceedings of IEEE Nuclear Science Symposium Conference Record, pp. 3402–3406.

Kuhn, A., Surti, S., Karp, J.S., Muehllehner, G., Newcomer, F.M., VanBerg, R., 2006. Performance Assessment of Pixelated $LaBr_3$ Detector Modules for Time-of-Flight PET. IEEE Trans. Nucl. Sci. 53 (3), 1090–1095.

Kuhn, A., Surti, S., Shah, K.S., Karp, J.S., 2005. Investigation of $LaBr_3$ Detector Timing Resolution. In: Proceedings of IEEE Nuclear Science Symposium Conference Record, pp. 2022–2026.

Van Loef, E.V.D., Dorenbos, P., Van Eijk, C.W.E., Kramer, K., Gudel, H.U., 2001. High-energy-resolution scintillator: Ce^{3+} activated $LaBr_3$. Appl. Phys. Lett. 79 (103), 1573–1575.

Menge, P.R., Gautier, G., Iltis, A., Rozsa, C., Solovyev, V., 2007. Performance of large lanthanum bromide scintillators. Nucl. Instrum. Methods Phys. Res. Sect. A: Accel. Spectrom. Detec. Assoc. Equip. A 579, 6–10.

Modamio, V., Valiente-Dobón, J.J., Jaworski, G., Hüyük, T., Triossi, A., Egea, J., Di Nitto, A., Söderström, P.-A., Agramunt Ros, J., de Angelis, G., de France, G., Erduran, M.N., Ertürk, S., Gadea, A., González, V., Kownacki, J., Moszynski, M., Nyberg, Palacz, M., Sanchis, E., Wadsworth, R., 2015. Digital pulse-timing

technique for the neutron detector array NEDA. Nucl. Instrum. Methods Phys. Res. Sect. A: Accel. Spectrom. Detect. Assoc. Equip. 775, pp. 71–76.
Naqvi, A.A., Al-Anezi, M.S., Kalakada, Z., AlMatouq, F.A., Maslehuddin, M., Gondal, M.A.,, Isab, A.A., Khateeb-ur, R., Dastageer, M., 2012a. Response tests of a $LaCl_3$:Ce scintillation detector with low energy prompt gamma-rays from boron and cadmium. Appl. Radiat. Isot. 70, 882–887.
Naqvi, A.A., Al-Matouq, F.A., Khiari, F.Z., Isab, A.A., Khateeb-ur Rehman, M.R., 2012b. Prompt gamma tests of $LaBr_3$:Ce and BGO detectors for detection of hydrogen, carbon and oxygen in bulk samples. Nucl. Instrum. Methods Phys. Res. Sect. A: Accel. Spectrom. Detect. Assoc. Equip. 684, 82–87.
Naqvi, A.A., Al-Anezi, M.S., Zameer, Kalakada, Isab, A.A., Raashid, M., Al Matouq, F.A., Khateeb-ur-Rehman, Khiari, F.Z., Garwan, M.A., Al-Amoudi, O.S.B., Maslehuddin, M., 2011. Detection efficiency of low levels of boron and cadmium with a $LaBr_3$: Ce scintillation detector. Nuclear Instruments and Methods in Physics Research A 665, 74–79.
Owens, A., Bos, A.J.J., Brandenburg, S., Dathy, C., Dorenbos, P., Kraft, S., Ostendorf, R. W., Ouspenski, V., Quarati, F., 2007. γ-Ray performance of a 1242 cm^3 $LaCl_3$:Ce scintillation spectrometer. Nucl. Instrum. Methods Phys. Res. Sect. A: Accel. Spectrom. Detect. Assoc. Equip. A574, 110–114.
Surti, S., Karp, J.S., Muehllehner, G., Raby, P.S., 2003. Investigation of Lanthanum Scintillators for 3-D PET. IEEE Trans. Nucl. Sci. 50 (3), 348–354.
Weele, D.N., ter., Schaart, D.R., Dorenbos, P., 2014. The Effect of Self-Absorption on the Scintillation Properties of Ce^{3+} Activated $LaBr_3$ and $CeBr_3$. IEEE Trans. Nucl. Sci. 61 (01), 683–688.